Frequency-resolved high-harmonic wavefront characterization

E. Frumker,[1,2,*] G. G. Paulus,[2,3] H. Niikura,[1,4] D. M. Villeneuve,[1] and P. B. Corkum[1,5]

[1]*Joint Laboratory for Attosecond Science, National Research Council of Canada and University of Ottawa, 100 Sussex Drive, Ottawa, ON K1A 0R6, Canada*
[2]*Department of Physics, Texas A&M University, College Station, Texas 77843, USA*
[3]*Institute of Optics and Quantum Electronics, Max-Wien-Platz 1, Jena 07743, Germany*
[4]*PRESTO, Japan Science and Technology Agency, 5 Sanbancho, Chiyodaku, Tokyo 102-0075, Japan*
[5] *paul.corkum@nrc.ca*
[*]*Corresponding author: eugene.frumker@nrc.ca*

Received August 11, 2009; accepted August 23, 2009;
posted September 9, 2009 (Doc. ID 115586); published September 30, 2009

We introduce and demonstrate a novel concept of frequency-resolved wavefront characterization. Our approach is particularly suitable for high-harmonic, extreme-UV (XUV) and soft X-ray radiation. The concept is based on an analysis of radiation diffracted from a slit scanned in front of a flat-field XUV spectrometer. With the spectrally resolved signal spread across one axis and the spatially resolved diffraction pattern in the other dimension, we reconstruct the wavefront. While demonstrated for high harmonics, the method is not restricted in wavelength. © 2009 Optical Society of America

OCIS codes: 120.5050, 020.2649, 260.1960.

It is as important to characterize the spatial properties of a high-harmonic (or attosecond) pulse, or of an x-ray free-electron laser beam, as it is to characterize its temporal properties. The high harmonics carry the combined signature of underlying quantum physical processes at the atomic level [1] and of the cooperative phase matching [2]. Accurate reconstruction of the high-harmonic spatial wavefront, along with its temporal profile, gives us a complete range of tools to apply to the fundamental quantum properties and dynamics associated with high-harmonic generation [3]. For many applications it will be necessary to accurately measure the beam properties, just as it is important to know the beam characteristics for many laser experiments. For example, high harmonics and attosecond pulses are being proposed as a front end for the next generation x-ray free-electron lasers. This oscillator-amplifier-like arrangement will require well-characterized high-harmonic sources [4–7].

From a laser perspective, characterizing extreme-UV (XUV) light is particular challenging. There are few high-quality optical components. Several methods for high-harmonic wavefront characterization have been reported. Point diffraction interferometry (PDI) [8], uses a semitransparent membrane plate with a small pinhole placed in front of the high-harmonic beam. The beam diffracting from the pinhole serves as a reference for a main beam transmitted through an aluminum film. This requires an extremely high optical-quality (on the scale of XUV radiation) membrane plate. An array of multiapertures in a Hartman-like sensor have also been used in combination with an aluminium filter [9]. Both approaches measure averaged wavefront across the full spectral bandwidth of the source. However, high-harmonic (and especially attosecond) pulses cover a very broad bandwidth, often spanning more than several octaves. This broad spectrum will smear the interference pattern. Smearing limits the existing technique to narrow-bandwidth radiation.

We present a concept of frequency-resolved wavefront characterization that is particularly suitable for characterizing XUV radiation. In keeping with tradition in the area [10] we give it an acronym—SWORD (Spectral Wavefront Optical Reconstruction by Diffraction). Our approach is based on an analysis of the diffraction pattern of a slit situated in front of a flat-field spectrometer. As the slit is scanned, the spectrally resolved diffraction pattern is recorded.

A schematic representation of our experiment is shown in Fig. 1. XUV radiation produced in a supersonic jet is diffracted through a horizontal scanning slit (SS) and then impinges onto the entrance slit (SE) of an XUV spectrometer outlined by the framed box. The vertically diffracted sample of the incoming wavefront passes through the spectrometer slit (SE). The spectrometer is constructed to resolve the spec-

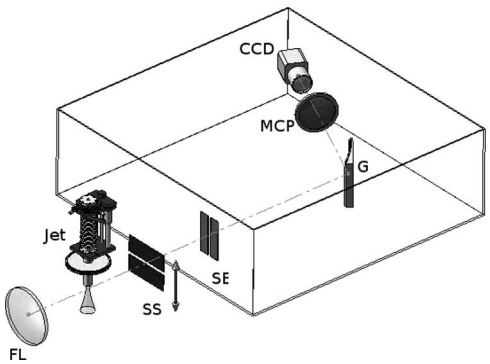

Fig. 1. Schematic of the experimental setup. The scanning slit (SS) is 20 μm wide, and the spectrometer slit (SE) width is 100 μm. The variable groove spacing flat field Hitachi imaging diffraction grating (model 001-0266) was used with nominal groove density of 1200 mm^{-1} [11].

trum in one direction (horizontal) and to allow essentially free-space field propagation in the other. Two-dimensional images are taken for each position of the scanning slit, producing what we call a diffractogram. The relative vertical position of the diffraction pattern's centroid is proportional to the wavefront slope of the sampled wavefront slice. Analyzing the measured diffractogram, we can reconstruct the wavefront using Eq. (1):

$$\delta_i = \delta z \frac{y_i - z_i}{d}. \tag{1}$$

In Eq. (1), y_i is the relative position of the centroid of the diffracted pattern, z_i is the relative slit position, d is the distance between the scanning slit and the imaging plane, δz is the scanning slit iteration step, and δ_i is the optical path difference across the slit. Then the sampled wavefront phase profile ϕ_n for the wavelength λ across the scanning direction is determined by

$$\phi_n = \frac{2\pi}{\lambda} \sum_{i=0}^{n} \delta_i. \tag{2}$$

The amplitude at each sampling point is determined by the integral intensity of the corresponding diffraction pattern in the diffractogram. The choice of the zero-phase point is arbitrary: it was chosen at the centroid of the intensity pattern. A different choice of the zero-phase point would correspond to a linear phase added to the reconstructed wavefront. This linear phase results in a spatial shift of the entire field pattern in the detection [multichannel plate (MCP)] plane.

The only assumption required for the validity of our approach is that the reconstructed wavefront is spatially coherent within the spectral resolution of the spectrometer. This is a less restrictive requirement as compared with the prerequisite for the conventional (Hartmann–Shack and interferometry-based) wavefront characterization techniques, which require spatial coherence over the full bandwidth of radiation. This makes SWORD applicable to a wide class of light sources.

In our experiment we have used high harmonics produced by focusing a 35 fs, ~400 μJ laser beam onto a nitrogen gas jet with a $f/\#=80$ lens. The laser beam was spatially filtered by propagating it through hollow fiber, and the radial symmetry of the mode was validated. The jet has 250 μm aperture and was operated with a backing pressure of 2.7 atm. Under these conditions we should see primarily short trajectory harmonics.

The imaging properties of our diffraction grating were studied in detail by Nakano *et al.* [12]. Based on their work, we estimated and confirmed experimentally resolution of our spectrometer to be 0.25 nm. A 40 mm diameter Burle imaging MCP was used in the imaging plane of the spectrometer, and the backside phosphor screen was imaged onto the CCD camera.

The typical high-harmonic spectrum, diffracted through the scanning slit, is shown on a log-scaled image in Fig. 2(a). As expected, we can clearly observe the sync-like diffraction structure from rectangular aperture in the vertical dimension, while the high harmonics are spectrally resolved in the horizontal dimension (harmonics 13 to 25 are shown). To be specific, we will choose harmonic 21 for further analysis. The small fragment of the sparse diffractogram (at 100 μm steps) for the 21th harmonic is shown in Fig. 2(b). In the experiment, a diffraction image was taken at each 20 μm step of the scanning slit. For each diffraction picture in the diffractogram, the centroid position and the integral intensity were found, after which the wavefront was reconstructed using Eqs. (1) and (2).

In the case of sources with rotational symmetry, the complete 2D wavefront profile can be reconstructed from a single vertical scan. There are several important high-harmonic sources that inherently have this symmetry, such as semi-infinite gas cells, hollow fibers, small gas cells, etc. In the most general case a complete 2D scan would be required (across the XUV beam +90 deg rotation to measure both projections).

Our jet source does not have rotational symmetry. However, it has reflection symmetry in the vertical plane. This implies that the normal to the wavefront lies in this plane. Therefore, to reconstruct the vertical wavefront profile, only one scan across this direction is needed. The phase and amplitude of the reconstructed wavefront profile are shown in Fig. 3(a).

In this example, we found the phase to be almost perfectly parabolic, corresponding to the divergent beam with a radius of curvature of 271 mm. For comparison, the distance between the gas jet and the scanning plane was 245±1 mm. In other words, the harmonics appear to originate before the jet, quanti-

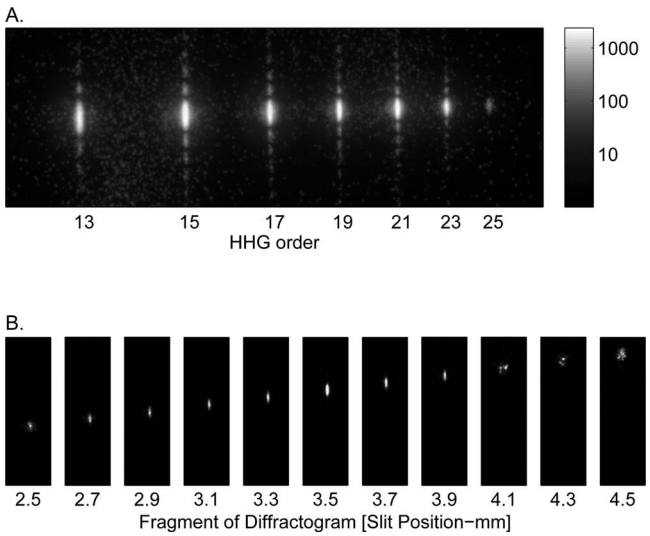

Fig. 2. (a) Logarithmic image of a high-harmonic spectrum diffracted through scanning slit. (b) The diffractogram. Each slice of the diffractogram shows the diffraction pattern for the particular scanning slit position printed below each slice. Only a small, sparse fragment of the complete diffractogram is shown. At each slice the intensity is normalized to maximum for the given slit position. In the experiment the slit was scanned and the diffraction pattern measured at 20 μm increments.

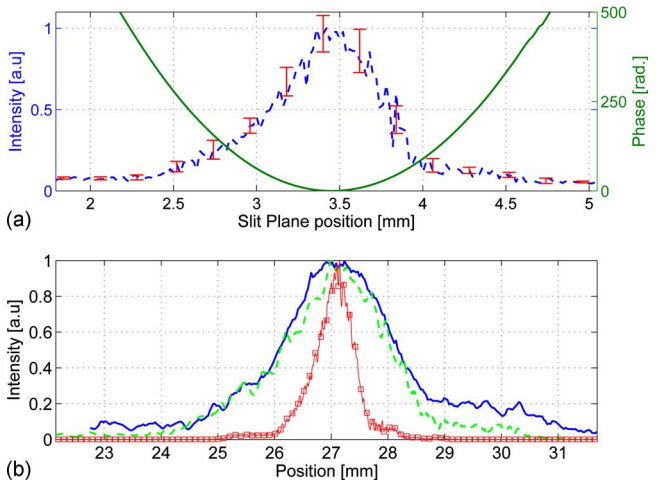

Fig. 3. (Color online) (a) Experimental results: phase and amplitude reconstruction of the 21st harmonic at the scanning slit position. Error bars for the reconstructed phase (~0.3%) are unobservable on the figure scale. (b) Intensity profile on the MCP plane. The solid curve shows the measured profile. The dashed curve represents reconstructed intensity. The reconstructed intensity profile for a flat phase is shown by the solid curve with markers in the center.

fying the phase structure placed on the beam by the radial intensity distribution of the fundamental. We repeated the scan measurements with different integration times. The phase reconstruction is repeatable to within 0.3%, even though the intensity noise (due to fluctuations in the laser power and the gas jet) was ~15%. Because the phase is measured from the centroid of the diffracted pattern it is not directly sensitive to amplitude fluctuations. Taking into account all relevant tolerances, we estimate the systematic error of our measurement to be better than 1%.

We have performed a similar reconstruction for all harmonics. The radius of curvature varies from 240 mm to 275 mm from harmonic 13 to harmonic 25. Referring to harmonic 21, the phase and amplitude profiles of the wavefront are shown in Fig. 3(a). We attribute the slight asymmetry in the amplitude of the wavefront profile to the density gradient of the jet in the vertical direction. This gradient result in varying density of molecules across the generating beam that influences both the harmonic generation process and the propagation of the fundamental beam.

To validate our results, we propagated the reconstructed wavefront profile from the scanning slit position to the imaging plane and compared the calculated profile with the high-harmonic profile measured without the scanning slit. We use the Fresnel transform [13] because the Fresnel number $D^2/Z\lambda \sim 25 \geq 1$, where $D \sim 700\ \mu$m is the high-harmonic extension size at the scanning slit position, $\lambda \simeq 38$ nm, and $Z=513$ mm is the distance between the scanning slit to the MCP. To account for the MCP and optical system resolution of 90 μm, we have convolved the numerically propagated field at the MCP position with the corresponding point spread function kernel. Both the measured and calculated profile are presented in [Fig. 3(b)]. For comparison, if we use only the amplitude information and assume a flat phase front, we find the central curve in the figure. It differs substantially from the measured results.

Because we know the size of our slit and relevant distances, we can compare the diffraction pattern with the theoretically expected sync function with shift. Doing so, we achieve at least two goals: first, a more accurate estimate of the linear term for the wavefront. Second, we can analyze the width of the sync function to estimate the quadratic term in the wavefront (phase variations across the slit). Thus we further increase the accuracy and/or reduce the number of the required sampling points.

In summary, we have demonstrated an approach of frequency-resolved wavefront characterization that is particularly suitable for characterization of high-harmonic and XUV radiation. The technique can be easily extended beyond the XUV spectral region. When combined with temporal characterization techniques [14,15], all information about the beam can be measured. This paves the way to temporal–spatial coupling studies of high-harmonic and attosecond pulses.

We are grateful for discussions and help of Andrei Naumov, Doug Moffatt, and Adrian Pegoraro. We acknowledge financial support of MURI grant W911NF-07-1-0475, Marie Curie IOF, and Japan Science and Technology Agency.

References

1. P. B. Corkum, Phys. Rev. Lett. **71**, 1994 (1993).
2. E. Constant, D. Garzella, P. Breger, E. Mevel, C. Dorrer, C. Le Blanc, F. Salin, and P. Agostini, Phys. Rev. Lett. **82**, 1668 (1999).
3. J. Itatani, J. Levesque, D. Zeidler, H. Niikura, H. Pepin, J. C. Kieffer, P. B. Corkum, and D. M. Villeneuve, Nature **432**, 867 (2004).
4. R. A. Bartels, A. Paul, H. Green, H. C. Kapteyn, M. M. Murnane, S. Backus, I. P Christov, Y. W. Liu, D. Attwood, and C. Jacobsen, Science **297**, 376 (2002).
5. R. Neutze, R. Wouts, D. van der Spoel, E. Weckert, and J. Hajdu, Nature **406**, 752 (2000).
6. W. L. Chao, B. D. Harteneck, J. A. Liddle, E. H. Anderson, and D. T. Attwood, Nature **435**, 1210 (2005).
7. H. M. Quiney, A. G. Peele, Z. Cai, D. Paterson, and K. A. Nugent, Nat. Phys. **2**, 101 (2006).
8. D. G. Lee, J. J. Park, J. H. Sung, and C. H. Nam, Opt. Lett. **28**, 480 (2003).
9. C. Valentin, J. Gautier, L. P. Goddet, C. Hauri, T. Marchenko, E. Papalazarou, G. Rey, S. Sebban, O. Scrick, P. Zeitoun, G. Dovillaire, X. Levecq, S. Bucourt, and M. Fajardo, J. Opt. Soc. Am. B **25**, B161 (2008).
10. D. J. Kane and R. Trebino, J. Quantum Electron. **29**, 571 (1993).
11. T. Kita, T. Harada, N. Nakano, and H. Kuroda, Appl. Opt. **22**, 512 (1983).
12. N. Nakano, H. Kuroda, T. Kita, and T. Harada, Appl. Opt. **23**, 2386 (1984).
13. J. W. Goodman, *Introduction to Fourier Optics* (McGraw-Hill, 1996).
14. P. M. Paul, E. S. Toma, P. Breger, G. Mullot, F. Auge, Ph. Balcou, H. G. Muller, and P. Agostini, Science **292**, 1689 (2001).
15. J. Itatani, F. Quéré, G. L. Yudin, M. Yu. Ivanov, F. Krausz, and P. B. Corkum, Phys. Rev. Lett. **88**, 173903 (2002).